Online supplementary material for

Outburst floods of the Maly Yenisei. Part II – New age constraints from Darhad basin

Jigjidsurengiin Batbaatar and Alan R. Gillespie

Quaternary Research Center, University of Washington, Seattle, WA, USA

Luminescence dating methods

Sample preparation. Coarse-grain extractions included wet sieving to separate the 150–212 μm grains, then treating with HCl to remove carbonates and with H_2O_2 to reduce organics. Quartz extraction involved treatment with 48% HF for 40 min followed by density separation of grains less than 2.67 specific gravity using a solution of lithium metatungstate. No HF etch was employed for feldspar extraction, which just involved density separation of grains <2.58 specific gravity. Individual grains were transferred onto specially milled disks by hand. We also prepared multi-mineral aliquots from the core sections where sand fraction was not available, extracting 1–8 μm fine sediments from the unexposed interior of the archive core. This was done by suspending the sediments in acetone for 2 min before retaining the suspended loads, and the sediments at the bottom after 20 min settling. The 20-min settling was done at least twice to insure the removal of all grains <1 μm. The samples were then transferred onto 1 cm stainless still disks by evaporating the acetone at 50°C.

Measurement and analysis. The luminescence from single grains of coarse quartz and feldspar was measured on a Risø DA-20 reader following the single-aliquot regenerative (SAR) protocol (Wintle and Murray 2006) modified for feldspars (Auclair *et al.* 2003). For quartz preheating of 240°C for 10 s after the regeneration doses and 200°C cut after the test doses was used; for feldspar preheating of 250°C for 1 min following both regeneration and test doses was used. Stimulation for single grains of quartz was with a 532 nm laser; for single grains of feldspar stimulation was with a 830 nm laser. Stimulation for multi-mineral aliquots used successive exposure to 470 nm and 870 nm LEDs. Emission for both quartz and multi-mineral aliquots was through 7.5 mm Hoya U-340 filters (UV). Emission for feldspar was through a blue filter pack (350–450 nm).

Pulsed measurements (Feathers *et al.* 2012) were done on fine grains from samples DBC1-79.6 and DBC1-9.15 to isolate the feldspar signals from quartz in the multi-mineral aliquots better. In pulsed OSL measurements the light stimulation is turned on and off, and luminescence is obtained during the off time, rather than during the stimulation as in the SAR protocol. The details on the procedure can be found in Feathers *et al.* (2012).

Fading assessment for the coarse-grained feldspars was conducted on single grains following Auclair *et al.* (2003) using the correction procedure of Huntley and Lamothe (2001). The multi-mineral analysis employed the double SAR method where the IR stimulation precedes the OSL stimulation (Banerjee *et al.* 2001). While the purpose of the IR stimulation is to reduce the feldspar signal, and therefore the fading signal, it may not remove this signal altogether. However, alpha efficiency factors, using the b-value system (0.6–0.7 Gy μm^2), were in the range of quartz for the OSL stimulation, so the OSL signal likely lacked a significant fading component (Janz *et al.* 2015).

The dose rates were assessed by thick source alpha counting and beta counting. We measured the moisture contents for the analysis. Dose rate conversions followed Adamiec and Aitken (1998). Cosmic dose determinations followed Prescott and Hutton (1994).

Calculation of ^{10}Be ages

We calculated ^{10}Be ages with CRONUS (version 2.2, Balco *et al.* 2008) using Heyman's (2014) globally calibrated ^{10}Be production rate of 3.99 ± 0.22 atoms g^{-1} yr^{-1} when referenced to the scaling of Stone (2000). For interpretation of the ages, we accepted the ages calculated with magnetic field-constant scaling scheme of Stone (2000), because the differences between ages calculated with various scaling schemes were less than the average 1σ measurement errors for individual sample (<10%). In Part 1 (Batbaatar and Gillespie 2015) we also updated the published ^{10}Be ages using the same calculation scheme. Gillespie *et al.* (2008) used a production rate of 5.9 atoms g^{-1} yr^{-1}; Arzhannikov *et al.* (2012) reported using 4.49 ± 0.29 atoms $g^{-1}yr^{-1}$; and Rother *et al.* (2014) used 4.43 ± 0.52 atoms g^{-1} yr^{-1} referenced to Dunai scaling (Dunai 2001). The sea-level production rates were scaled to the latitude and altitude of the sampling sites, with corrections for the sample thickness and topographic shielding in the CRONUS calculator.

Sensitivity of ^{10}Be ages to erosion

In calculating apparent ^{10}Be ages, we assumed that boulder erosion had been negligible. Although we sampled apparently uneroded rocks, mainly deposited on the most recent (local last glacial maximum (LGM), or LGM_L) moraines, evidence of boulder erosion on pre-LGM_L moraines in northern Mongolia (e.g. at the Högiin and Jombolok rivers) suggests that slow erosion does occur there, and our calculated ages are therefore minima. To test the sensitivity of the CRE ages to erosion, we recalculated the ages assuming that the boulder erosion rate was up to 0.5 cm ka^{-1} (e.g. Nichols *et al*. 2006).

The calculated exposure ages of Table S1 corrected for erosion are shown in Table S2 and summarized graphically in Figure S1. Exposure ages of 30 ka that we report in Table S1 are as much as 4.5 ka too young, if erosion was at 0.5 cm ka^{-1}. The erosion of ≥0.4 cm ka^{-1} in some of the old samples would have been enough to balance the fresh production of ^{10}Be, so that the concentration does not increase with age. Therefore, the concentration of ^{10}Be "saturates" and it becomes impossible to calculate an apparent age greater than those for surfaces with lower erosion rates, regardless of the actual age.

Sensitivity of ^{10}Be ages to neutron shielding by snow

The ^{10}Be ages reported in Table S1 have not been corrected for shielding by persistent snow cover. Although the studied moraines were between latitudes 45°N and 53°N, Mongolia is in the arid interior of Asia. Modern annual precipitation in northern Mongolia at the elevations of the glacier termini (~1550 m asl) is 430 mm, ~65% of which is ephemeral summertime snow or rain (CRU 2.0 data: Mitchell and Philip 2005). Conditions were drier and colder there during the LGM, with ~10–50% less precipitation based on the lake-level depression for Hövsgöl lake (Prokopenko *et al*. 2005), and a ~5 K decrease in temperature based on the equilibrium-line altitude depression of ~900 m around Darhad basin (Gillespie *et al*. 2008). A 4-month per year snowpack of 250 mm depth (density 0.3 g cm^{-3}) would increase the exposure age by 2% (Gosse and Phillips 2001), accounting for ~0.4 ka increase in apparent age for global LGM (MIS 2) landforms.

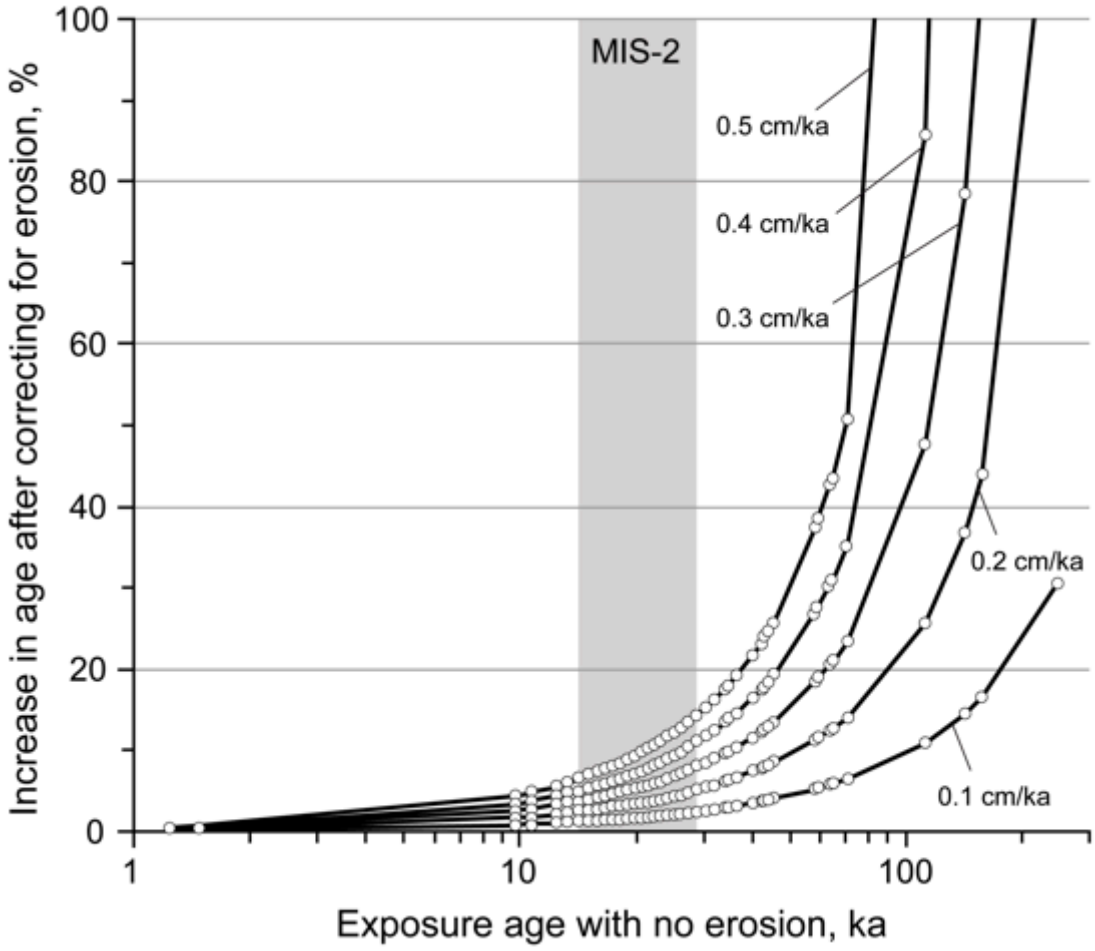

Figure S1. Potential increase in the apparent exposure ages (circles) after correcting for various erosion rates. The population includes the new and literature dates from Gillespie *et al*. (2008), Arzhannikov *et al*. (2012), and Rother *et al*. (2014). The increase of the ages by more than 100% is excluded in the plot. The percent increases of the ^{10}Be ages after correction are given in Table S2.

Table S1. ^{10}Be exposure ages (in ka ± 1σ) for the new samples summarized in Figure 11 in the main text calculated using various scaling schemes for spallation. St: Lal (1991)/Stone (2000); De: Desilets and Zreda (2003) and Desilets *et al*. (2006); Du: Dunai (2001); Li: Lifton *et al*. (2005); Lm: Time-dependent Lal (1991)/Stone (2000). The ages shown in bold (St) are discussed in the text. The maximum difference for MIS 2 samples is ~0.8 ka.

Sample ID	**St**	De	Du	Li	Lm
070402-AG-RMS-1	**12.3 ± 0.9**	12.0 ± 1.1	12.1 ± 1.0	11.7 ± 1.0	12.5 ± 0.9
070402-AG-RMS-2-47	**12.3 ± 0.8**	12.0 ± 1.0	12.1 ± 0.9	11.7 ± 0.9	12.5 ± 0.8
070402-AG-RMS-2-64	**13.0 ± 0.9**	12.6 ± 1.0	12.7 ± 1.0	12.3 ± 0.9	13.1 ± 0.8
070402-AG-RMS-3-47	**10.7 ± 0.7**	10.3 ± 0.8	10.4 ± 0.8	10.1 ± 0.8	10.9 ± 0.7
070402-AG-RMS-3-64	**10.5 ± 0.7**	10.2 ± 0.9	10.2 ± 0.8	9.9 ± 0.8	10.7 ± 0.7
070402-AG-RMS-4	**10.4 ± 0.8**	10.1 ± 0.9	10.1 ± 0.9	9.8 ± 0.8	10.6 ± 0.8
070402-AG-RMS-5	**9.7 ± 0.7**	9.4 ± 0.8	9.5 ± 0.8	9.2 ± 0.8	9.9 ± 0.7
070402-AG-RMS-6	**1.5 ± 0.1**	1.5 ± 0.2	1.5 ± 0.2	1.4 ± 0.2	1.5 ± 0.2
070402-AG-RMS-7	**1.2 ± 0.1**	1.2 ± 0.1	1.2 ± 0.1	1.2 ± 0.1	1.3 ± 0.1
070402-AG-RMS-8A	**26.4 ± 1.7**	25.3 ± 2.0	25.4 ± 1.9	24.4 ± 1.8	26.5 ± 1.6
070402-AG-RMS-8B	**20.1 ± 1.3**	19.4 ± 1.5	19.5 ± 1.5	18.8 ± 1.4	20.3 ± 1.2
070402-AG-RMS-9	**28.4 ± 1.8**	27.3 ± 2.1	27.4 ± 2.1	26.3 ± 1.9	28.6 ± 1.7
070802-AG-RSLK-1	**20.9 ± 1.5**	21.3 ± 1.8	21.5 ± 1.8	20.8 ± 1.6	21.1 ± 1.4
070802-AG-RSLK-2	**22.7 ± 1.6**	23.2 ± 2.0	23.4 ± 1.9	22.6 ± 1.8	22.9 ± 1.5
070802-AG-RSLK-3	**20.6 ± 1.4**	21.1 ± 1.8	21.2 ± 1.7	20.6 ± 1.6	20.8 ± 1.4
070802-AG-RSLK-4	**64.4 ± 4.3**	65.5 ± 5.3	65.5 ± 5.2	63.3 ± 4.7	64.5 ± 4.0
070802-AG-RSLK-5	**20.0 ± 1.4**	20.4 ± 1.7	20.6 ± 1.7	19.9 ± 1.6	20.1 ± 1.3
070802-AG-RSLK-6	**14.1 ± 1.0**	14.5 ± 1.2	14.6 ± 1.2	14.2 ± 1.1	14.3 ± 1.0
070802-AG-RSLK-7	**16.5 ± 1.1**	16.8 ± 1.4	17.0 ± 1.3	16.5 ± 1.2	16.6 ± 1.0
070802-AG-RSLK-8	**12.4 ± 1.3**	12.8 ± 1.5	12.9 ± 1.5	12.6 ± 1.4	12.6 ± 1.3
070802-AG-RSLK-10	**18.7 ± 1.3**	19.2 ± 1.6	19.3 ± 1.6	18.7 ± 1.5	18.9 ± 1.3
071002-AG-RDJO-1	**19.8 ± 1.4**	20.3 ± 1.7	20.4 ± 1.7	19.8 ± 1.6	20.0 ± 1.4
071002-AG-RDJO-2	**20.8 ± 1.5**	21.2 ± 1.8	21.4 ± 1.8	20.7 ± 1.6	20.9 ± 1.4
071002-AG-RDJO-3	**34.5 ± 3.0**	35.2 ± 3.4	35.3 ± 3.4	34.1 ± 3.2	34.6 ± 2.9
071002-AG-RDJO-5	**23.0 ± 2.1**	23.5 ± 2.4	23.6 ± 2.4	22.9 ± 2.2	23.1 ± 2.0
071002-AG-RDJO-6	**18.8 ± 1.3**	19.3 ± 1.6	19.4 ± 1.6	18.8 ± 1.4	19.0 ± 1.2
071202-AG-ROKA-6	**16.5 ± 1.2**	16.8 ± 1.5	17.0 ± 1.4	16.5 ± 1.3	16.6 ± 1.2
080709-HA-JB-02	**36.1 ± 2.3**	35.3 ± 2.3	35.3 ± 2.7	33.9 ± 2.4	36.1 ± 2.1
080709-HA-JB-03	**34.0 ± 2.5**	33.3 ± 2.9	33.3 ± 2.8	32.0 ± 2.6	34.1 ± 2.4
150707-DB-AG-003A	**23.8 ± 1.5**	24.2 ± 1.9	24.4 ± 1.8	23.6 ± 1.7	24.0 ± 1.4
150707-DB-AG-003C	**20.7 ± 1.4**	21.0 ± 1.7	21.2 ± 1.7	20.6 ± 1.5	20.8 ± 1.3
ZAG-ARG-01A	**24.4 ± 1.6**	23.5 ± 1.9	23.6 ± 1.9	23.1 ± 1.7	24.2 ± 1.5
ZAG-ARG-01B	**20.2 ± 1.3**	19.6 ± 1.5	19.7 ± 1.5	19.3 ± 1.4	20.1 ± 1.2
ZAG-ARG-02B	**17.2 ± 1.2**	17.0 ± 1.4	17.1 ± 1.4	16.8 ± 1.3	17.2 ± 1.1
ZAG-ARG-03A	**22.6 ± 1.8**	22. ± 12.1	22.3 ± 2.0	21.8 ± 1.9	22.5 ± 1.7
ZAG-ARG-03B	**158.3 ± 11.4**	150.4 ± 13.1	150.6 ± 12.7	145.2 ± 11.7	154.1 ± 10.6
ZAG-ARG-04B	**27.6 ± 1.8**	26.7 ± 2.2	26.8 ± 2.1	26.2 ± 2.0	27.3 ± 1.7
ZAG-SB-04A	**30.0 ± 1.9**	29.0 ± 2.3	29.1 ± 2.2	28.4 ± 2.0	29.7 ± 1.7
ZAG-SB-04B	**58.5 ± 3.5**	55.9 ± 4.3	56.0 ± 4.1	54.2 ± 3.8	57.5 ± 3.2
ZAG-SB-04C	**24.5 ± 1.5**	23.8 ± 1.9	23.9 ± 1.8	23.4 ± 1.7	24.3 ± 1.4
ZAG-SB-05	**158.1 ± 9.8**	149.4 ± 11.7	149.61 ± 1.3	144.1 ± 10.2	154.0 ± 8.8

Table S2. Increase in the calculated exposure ages after correcting for various erosion rates. Tabulated samples are those newly dated for this paper. Exposure ages are calculated using the time-constant spallation scaling scheme of Stone (2000). The highest erosion rate of 0.5 cm ka^{-1} will decrease an uncorrected MIS 2 ages by 4 ka at most.

Sample ID	Exposure age with no erosion (ka ± 1σ)	% Increase in age for various erosion rates				
		0.1 cm ka^{-1}	0.2 cm ka^{-1}	0.3 cm ka^{-1}	0.4 cm ka^{-1}	0.5 cm ka^{-1}
070402-AG-RMS-1	12.3 ± 0.9	1.1	2.1	3.2	4.4	5.5
070402-AG-RMS-2-47	12.3 ± 0.8	1.0	2.1	3.2	4.4	5.5
070402-AG-RMS-2-64	13.0 ± 0.9	1.1	2.3	3.5	4.7	6.0
070402-AG-RMS-3-47	10.7 ± 0.7	0.9	1.8	2.8	3.8	4.8
070402-AG-RMS-3-64	10.5 ± 0.7	0.9	1.8	2.8	3.7	4.7
070402-AG-RMS-4	10.4 ± 0.8	0.9	1.8	2.7	3.7	4.6
070402-AG-RMS-5	9.7 ± 0.7	0.8	1.7	2.5	3.4	4.3
070402-AG-RMS-6	1.5 ± 0.1	0.1	0.3	0.4	0.5	0.7
070402-AG-RMS-7	1.2 ± 0.1	0.1	0.2	0.3	0.4	0.5
070402-AG-RMS-8A	26.4 ± 1.7	2.3	4.7	7.3	10.0	13.0
070402-AG-RMS-8B	20.1 ± 1.3	1.7	3.5	5.4	7.4	9.5
070402-AG-RMS-9	28.4 ± 1.8	2.5	5.1	7.9	11.0	14.2
070802-AG-RSLK-1	20.9 ± 1.5	1.8	3.6	5.6	7.7	9.8
070802-AG-RSLK-2	22.7 ± 1.6	1.9	4.0	6.1	8.4	10.8
070802-AG-RSLK-3	19.8 ± 1.4	1.8	3.6	5.5	7.5	9.7
070802-AG-RSLK-4	64.4 ± 4.3	5.8	12.6	20.8	30.7	43.4
070802-AG-RSLK-5	20.0 ± 1.4	1.7	3.5	5.3	7.3	9.3
070802-AG-RSLK-6	14.1 ± 1.0	1.2	2.4	3.7	5.0	6.4
070802-AG-RSLK-7	16.5 ± 1.1	1.4	2.8	4.3	5.9	7.5
070802-AG-RSLK-8	12.4 ± 1.3	1.0	2.1	3.2	4.4	5.5
070802-AG-RSLK-10	18.7 ± 1.3	1.6	3.3	5.0	6.8	8.7
071002-AG-RDJO-1	19.8 ± 1.4	1.7	3.4	5.3	7.2	9.3
071002-AG-RDJO-2	20.8 ± 1.5	1.8	3.6	5.6	7.6	9.8
071002-AG-RDJO-3	34.5 ± 3.0	3.0	6.2	9.7	13.6	17.8
071002-AG-RDJO-5	23.0 ± 2.1	2.0	4.0	6.2	8.5	11.0
071002-AG-RDJO-6	18.8 ± 1.3	1.6	3.3	5.0	6.8	8.7
071202-AG-ROKA-6	16.1 ± 1.2	1.4	2.8	4.3	5.9	7.5
080709-HA-JB-02	36.1 ± 2.3	3.1	6.6	10.3	14.5	19.1
080709-HA-JB-03	34.0 ± 2.5	3.0	6.2	9.7	13.5	17.7
150707-DB-AG-003A	23.8 ± 1.5	2.0	4.2	6.5	8.9	11.5
150707-DB-AG-003C	20.7 ± 1.4	1.8	3.6	5.5	7.6	9.7
ZAG-ARG-01A	24.4 ± 1.6	2.1	4.3	6.7	9.2	11.8
ZAG-ARG-01B	20.2 ± 1.3	1.7	3.5	5.4	7.4	9.5
ZAG-ARG-02B	17.2 ± 1.2	1.5	3.0	4.6	6.2	8.0
ZAG-ARG-03A	22.6 ± 1.8	1.9	4.0	6.1	8.4	10.8
ZAG-ARG-03B	158.3 ± 11.4	16.6	43.9	105.1	saturated	saturated
ZAG-ARG-04B	27.6 ± 1.8	2.4	4.9	7.6	10.5	13.7
ZAG-SB-04A	30.0 ± 1.9	2.6	5.4	8.4	11.6	15.1
ZAG-SB-04B	58.5 ± 3.5	5.3	11.4	18.5	27.1	37.6
ZAG-SB-04C	24.5 ± 1.5	2.1	4.3	6.7	9.2	11.9
ZAG-SB-05	158.1 ± 9.8	16.6	43.9	105.1	saturated	saturated

Table S3. Diatom species in the lake sediments from the DBC1 core.

Diatom species	Number of diatoms per slide at each 10-cm depth interval (m)[a,b]							
	78.95	79.05	79.15	79.25	79.35	79.45	79.55	79.75
Achnanthes lanceolata	10	-	-	-	-	-	-	-
Amphora ovalis	-	5	4	4	-	-	-	-
Cocconeis placentula	-	-	1	-	2	-	-	-
Cocconeis sp.	-	-	-	-	-	1	-	-
Cyclotella ocellata[c]	-	19	55	14	-	-	-	-
Cymbella cf. aspera	-	-	-	-	-	1	-	-
Cymbella inaequalis	-	-	-	-	-	2	-	-
Cymbella minuta	1	18	16	5	9	6	-	2
Cymbella sp.	-	-	-	-	-	3	-	-
Diploneis ovalis	-	1	4	1	-	-	-	-
Epithemia sp.	-	-	1	-	-	-	-	-
Epithemia turgida	-	-	-	1	-	-	-	-
Fragilaria constricta	13	1	2	-	-	-	-	-
Fragilaria construens[c]	192	8	25	122	43	190	-	9
Fragilaria pinnata	-	-	-	1	-	3	-	-
Gomphonema acuminatum	-	-	-	-	-	2	-	-
Gomphonema sp.	-	1	1	1	-	-	-	-
Gomphonema subtile	-	-	16	5	-	-	-	-
Luticola mutica	-	3	-	-	-	1	-	-
Navicula digitoradiata	-	7	5	2	-	1	-	-
Navicula mutica	-	-	-	-	-	1	-	-
Navicula radiosa	-	3	-	4	-	-	-	-
Navicula sp.	-	-	-	3	-	-	-	-
Nitzschia sp.	-	-	1	1	-	-	-	1
Planothidium delicatulum[c]	7	155	70	56	171	23	200+	200+
Parlibellus sp.	-	4	3	-	-	-	-	-
Pinnularia cf. viridis	-	-	1	-	-	-	-	-
Sellaphora pupula var. rectangularis	-	4	-	2	-	-	-	-
Stephanodiscus sp.	-	1	-	-	-	1	-	-
Synedra sp.	-	-	1	-	-	-	-	-
Tabellaria cf. lacustris	-	-	-	4	-	-	-	-
Tabellaria cf. ventricosa	-	-	4	-	-	-	-	-
Tetracyclus cf. lacustris	2	6	-	-	-	4	-	-
Unknown	-	4	10	2	2	2	-	-
Cysts[d]	-	-	-	-	2	-	3	-

[a] Depths of the beginning of each 10-cm increment are shown.

[b] No diatoms were found at the depth of 79.00 m.

[c] Species names in bold are discussed in the main text.

[d] The cysts are not specific to particular species.

Modern ELA and climate in the vicinity of Darhad basin

The dating of some of the moraines from Darhad basin so far has been problematical (cf. Gillespie et al., 2008). Only a handful of ^{10}Be ages have been determined for each moraine, and for some moraines the ages have scattered greatly relative to their precisions, likely due to geological complications such as inheritance and/or solifluction that were not recognized during sampling. Telecorrelation with nearby dated moraines from the same glaciation could improve our confidence in the ages, except that relative dating and soil development may not be trustworthy indicators of surface age in areas of permafrost, such as northern Mongolia, and the age of the LGM_L itself appears to vary significantly from place to place in Central Asia on a scale of 500 km or more (Koppes *et al*. 2008; Rupper *et al.* 2009). Therefore, the best approach for telecorrelating the moraine ages is to limit the telecorrelation between moraines to separations less than 500 km, and to limit comparisons to moraines having the same equilibrium-line altitude (ELAs), assuming that ELAs that differ by no more than the technique precision (~100 m: e.g., Meierding 1982; Gillespie 1991) probably refer to the same climatic episode, and that the numerical ages for the different moraines can be grouped to improve their reliability.

However, before correlating moraines in northern Mongolia it is necessary first to establish the scale of climatic variability there, since the ~500 km scale from Rupper *et al.* (2009) was imposed by the resolution of the climate models they had access to. To do this, we first estimated ELAs for moraine sequences for a few hundred km around Darhad basin, and then fit trend lines to them. We argue that if the trend lines show no erratic fluctuations such as observed by Rupper *et al*. (2009) it is helpful to assess timing of maximum glacial extents for Darhad in the context of chronosequences for the surrounding mountain ranges.

For this purpose, we dated moraine sequences near the highest peak of the East Sayan ice field, Mönh Saridag, which hosts a small active cirque glacier. We also dated moraine sequences in the Jombolok, Sailag, and Oka river valleys to determine a chronosequence for the East Sayan ice field independent of the Tengis glaciers. Komatsu *et al.* (2009) proposed another location for an ice dam on the Maly Yenisei – the outlet glacier that descended the Hadar Üüs river valley, west of the Hoit Aguy massif (Figure 2). We present a new ^{10}Be age for a moraine in Hoit Aguy, which was not covered by the East Sayan ice field, in order to provide local control on the ELA for the glacier, and to estimate the local ELA independent of complicating factors due to the ice field itself. To the south, ~300 km from Darhad basin, we dated moraine sequences near Gyalgar peak to help provide the regional pattern of glacial extents during MIS 2.

The modern climate in the vicinity (~1000 km) of Darhad basin is described from the reanalysis climate data (CRU TS version 3.23; Harris *et al.* 2014) and shown in Figures S2 and S3. The annual precipitation decreases with latitude in the vicinity of Darhad basin. There is no apparent correlation between the precipitation and longitude. In the region, 50–70% of the annual precipitation falls in summer, suggesting a similar accumulation regime of the glaciers there (Figure S2 c, d; Sakai *et al.* 2015).

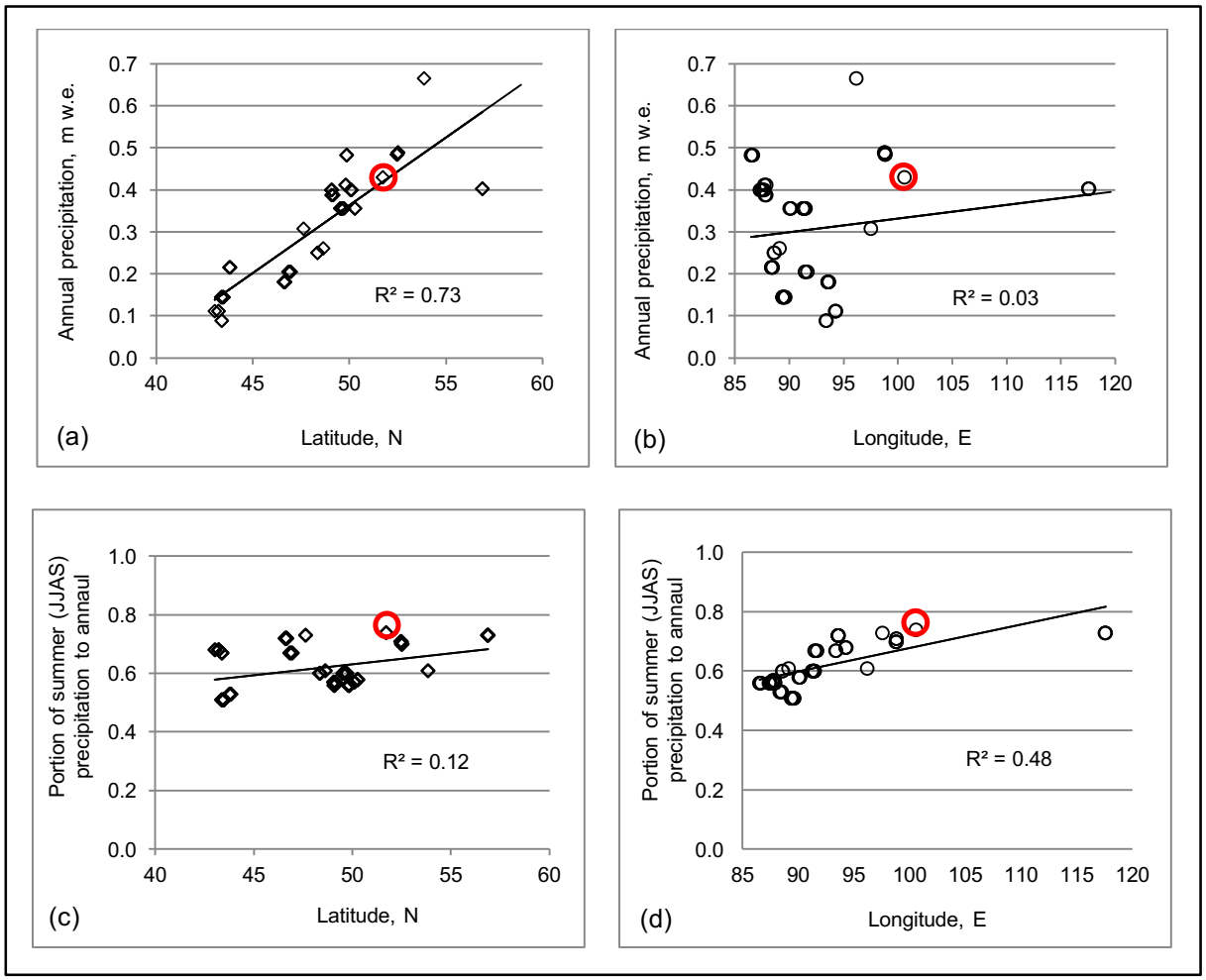

Figure S2. The relationship between the latitude and longitude and the precipitation in the vicinity of Darhad basin, showing the annual precipitation rate (w.e = water equivalent) in relation to (a) latitude and (b) longitude. The portion of summer (JJAS) precipitation is shown in relation to (c) latitude and (d) longitude. The precipitation data are for the 0.5° grid of the CRU data (Harris *et al*. 2014) that includes the mountain range with the calculated ELA. R^2 refers to the correlation coefficient for the linear regression line. The red circle shows the data for the modern glacier on Mönh Saridag, the peak closest to Darhad basin.

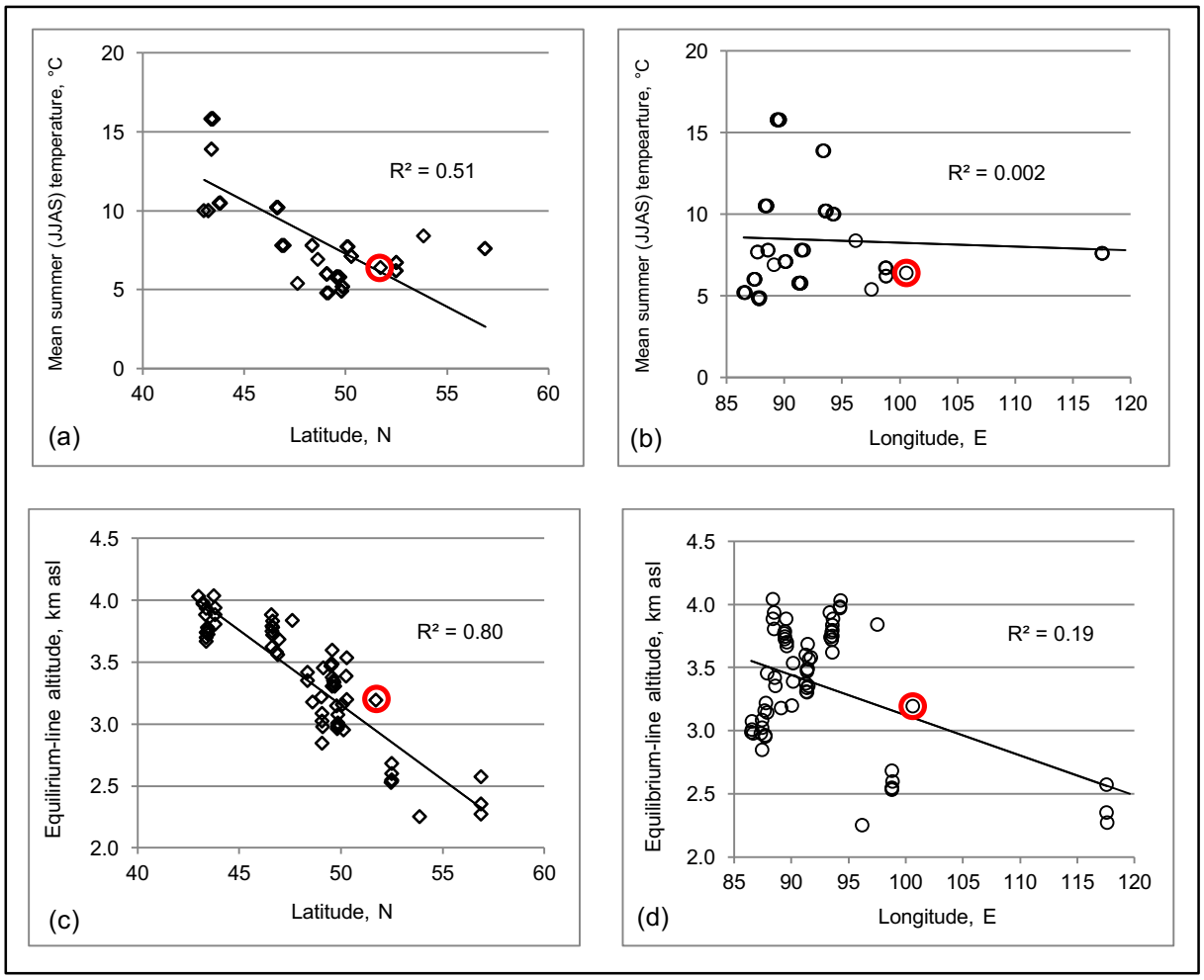

Figure S3. Summer (JJAS) temperature and the ELA in the vicinity of Darhad basin. The summer temperature is shown in relation to (a) latitude and (b) longitude. ELA is shown in relation to (c) latitude and (d) longitude. The precipitation data are for the 0.5° grid of the CRU data (Harris *et al*. 2014) that includes the mountain range with the calculated ELA. R^2 refers to the correlation coefficient for the linear regression line. The red circle shows the data for the modern glacier on Mönh Saridag, the peak closest to Darhad basin.

Summer temperature increases with the lowering of latitude (Figure S3 a). The ELA corresponds strongly to this trend, lowering at a rate ~150 m per degree of decrease in latitude (Figure S3 c). There is no apparent correlation between the summer temperature and longitude (Figure S3 b), which results the similar low variability of ELA with longitude. The air temperature is regulated by solar insolation as a function of latitude and the strong correlation between summer temperature and the ELA suggests that the glaciers in the mountain ranges within ~1000 km of Darhad basin respond mostly to changes in temperature. The ELA and the precipitation for the same showed no correlation ($R^2 = 0.06$), suggesting that the glaciers in the region do not vary much due to changes in precipitation.

Table S4. The equilibrium-line altitude for modern glaciers and the mean (1901 – 1931) climate parameters in the vicinity of Darhad basin

Assigned name	Latitude, degrees N	Longitude, degrees E	ELA (THAR=0.58), m asl	Mean annual PPT, mm	Mean summer (JJAS) temperature, °C	Portion of summer (JJAS) PPT, %
Aktru glacier	50.122308	87.714013	2955	400	7.7	57
Barkol Shan	43.396359	93.421594	3742	89	13.9	67
Barkol Shan	43.391621	93.360286	3938	89	13.9	67
Belukha peak	49.861533	86.659125	2980	482	5.2	56
Belukha peak	49.842899	86.498465	2990	482	5.2	56
Belukha peak	49.851076	86.580478	3078	482	5.2	56
Belukha peak	49.851076	86.580478	3012	482	5.2	56
Bogd peak	43.825056	88.496799	3940	215	10.5	53
Bogd peak	43.813125	88.501683	3808	215	10.5	53
Bogd peak	43.817914	88.372126	3885	215	10.5	53
Bogd peak	43.770951	88.356579	4041	215	10.5	53
Bolshoy Aktru	50.063454	87.689233	3159	400	7.7	57
Border area	49.057638	87.793280	3221	387	4.8	57
Dayan nuur	48.351140	88.629313	3355	250	7.8	60
Dayan nuur	48.356373	88.569547	3422	250	7.8	60
East Bogd	43.469190	89.385254	3773	144	15.8	51
East Bogd	43.460639	89.406934	3785	144	15.8	51
East Bogd	43.460635	89.406951	3748	144	15.8	51
East Bogd	43.463022	89.435862	3728	144	15.8	51
East Bogd	43.367011	89.565573	3887	144	15.8	51
East Bogd	43.384498	89.627163	3701	144	15.8	51
East Bogd	43.378960	89.614013	3671	144	15.8	51
Grandiozniy	53.856739	96.178077	2253	664	8.4	61

Table S4 (continued)

Assigned name	Latitude, degrees N	Longitude, degrees E	ELA (THAR=0.58), m asl	Mean annual PPT, mm	Mean summer (JJAS) temperature, °C	Portion of summer (JJAS) PPT, %
Harhiraa	49.589676	91.251310	3602	356	5.8	60
Harhiraa	49.531142	91.439718	3493	356	5.8	60
Harhiraa	49.587889	91.392292	3309	356	5.8	60
Harhiraa	49.589676	91.251310	3379	356	5.8	60
Harhiraa	49.524000	91.396645	3472	356	5.8	60
Harhiraa	49.575957	91.398259	3487	356	5.8	60
Kanas river	49.083478	87.468999	3088	400	6.0	56
Kanas river	49.083478	87.468999	3026	400	6.0	56
Kanas river	49.083478	87.468999	2848	400	6.0	56
Kanas river	49.100891	87.339603	2982	400	6.0	56
Kara oyuk river	49.796303	87.909607	3148	412	4.9	56
Möngön Taiga	50.278836	90.066643	3199	355	7.1	58
Möngön Taiga	50.285085	90.135820	3536	355	7.1	58
Möngön Taiga	50.269810	90.146286	3390	355	7.1	58
Mönh Hairhan	46.837444	91.698230	3584	205	7.8	67
Mönh Hairhan	46.961590	91.447763	3687	205	7.8	67
Mönh Hairhan	46.902992	91.526653	3565	205	7.8	67
Mönh Saridag	51.722757	100.600457	3194	430	6.4	74
Otgontenger	47.620185	97.535583	3843	308	5.4	73
Sutai	46.663988	93.552129	3783	181	10.2	72
Sutai	46.625774	93.600142	3795	181	10.2	72
Sutai	46.628266	93.597447	3752	181	10.2	72
Sutai	46.652719	93.553588	3723	181	10.2	72
Sutai	46.612811	93.564922	3623	181	10.2	72
Sutai	46.605113	93.651510	3886	181	10.2	72
Sutai	46.643772	93.600827	3836	181	10.2	72
Taldur glacier	49.817514	87.716003	2968	412	4.9	56
Potanin glacier	49.154196	87.874787	3459	387	4.8	57
Tomort peak	43.214871	94.239697	3972	111	10.0	68
Tomort peak	43.214871	94.239697	3983	111	10.0	68
Tomort peak	43.021123	94.304215	4034	111	10.0	68
Topografov peak-North	52.517122	98.773056	2684	488	6.7	70
Topografov peak-North	52.516565	98.809538	2550	488	6.7	70
Topografov peak-North	52.507467	98.808292	2543	488	6.7	70
Topografov peak-South	52.499411	98.839464	2602	483	6.2	71
Topografov peak-South	52.466862	98.795974	2534	483	6.2	71
Transbaikalia	56.880323	117.520653	2576	402	7.6	73
Transbaikalia	56.877943	117.540413	2357	402	7.6	73
Transbaikalia	56.887536	117.577484	2275	402	7.6	73
Tsengel Hairhan	48.625752	89.112385	3182	260	6.9	61
Turgen peak	49.664062	91.368397	3341	356	5.8	60
Turgen peak	49.654316	91.484847	3355	356	5.8	60
Turgen peak	49.716592	91.342580	3310	356	5.8	60

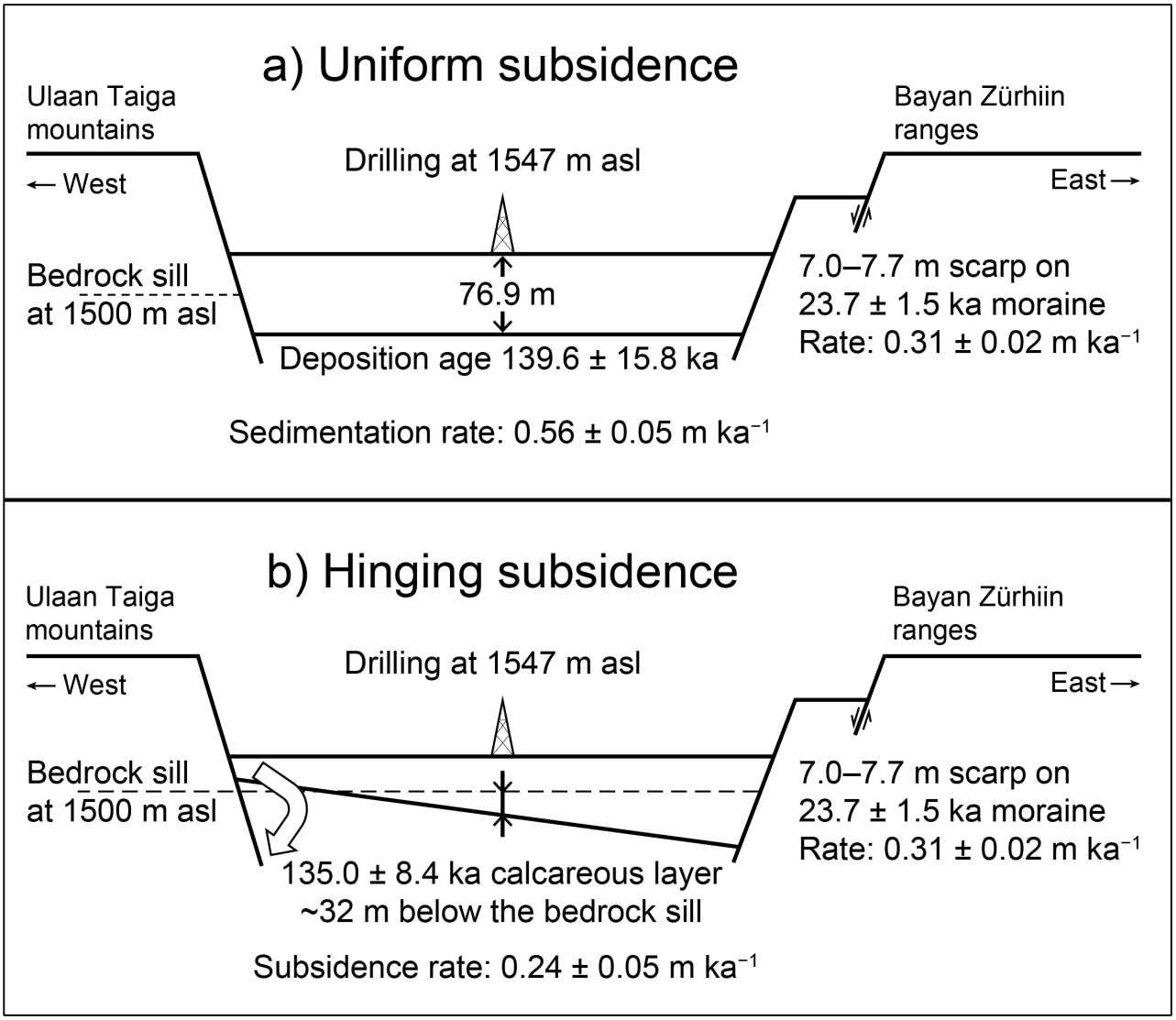

Figure S4. Two alternative models for subsidence of the Darhad basin floor. a) Uniform subsidence assumes the same rate applies everywhere; b) Hinging subsidence assumes faster rates on the east than in the west. The subsidence rate would be intermediate in the middle of the basin. The fault scarps on the east side are more distinct and/or larger than on the west.

References cited in the supplementary online material

Adamiec, G., and Aitken, M., 1998, Dose-rate conversion factors: update: Ancient TL, v. 16, no. 2, p. 37–50.

Arzhannikov, S.G., Braucher, R., Jolivet, M., Arzhannikova, A.V., Vassallo, R., Chauvet, A., Bourlès, D., and Chauvet, F., 2012, History of late Pleistocene glaciations in the central Sayan-Tuva Upland (southern Siberia): Quaternary Science Reviews, v. 49, p. 16-32.

Auclair, M., Lamothe, M., and Huot, S., 2003, Measurement of anomalous fading for feldspar IRSL using SAR: Radiation Measurements, v. 37, p. 487–492.

Balco, G., Stone, J.O., Lifton, N.A., and Dunai, T.J., 2008, A complete and easily accessible means of calculating surface exposure ages or erosion rates from ^{10}Be and ^{26}Al measurements: Quaternary Geochronology, v. 3, p. 174–195.

Banerjee, D., Murray, A.S., Bøtter-Jensen, L., and Lang, A., 2001, Equivalent dose estimation using a single aliquot of polymineral fine grains: Radiation Measurements, v. 33(1), p. 73–94.

Batbaatar, J., and Gillespie, A.R., 2015, Outburst floods of the Maly Yenisei. Part 1: International Geology Review, DOI:10.1080/00206814.2015.1114908.

Desilets, D., and Zreda, M., 2003, Spatial and temporal distribution of secondary cosmic-ray nucleon intensities and applications to in-situ cosmogenic dating: Earth and Planetary Science Letters, v. 206, p. 21–42.

Desilets, D., Zreda, M., and Prabu, T., 2006, Extended scaling factors for in situ cosmogenic nuclides: new measurements at low latitude: Earth and Planetary Science Letters, v. 246, p. 265–276.

Dunai, T., 2001, Influence of secular variation of the geomagnetic field on production rates of in situ produced cosmogenic nuclides: Earth and Planetary Science Letters, v. 193, p. 197–212.

Feathers, J.K., Casson, M.A., Schmidt, A.H., and Chithambo, M.L., 2012, Application of pulsed OSL to polymineral fine-grained samples: Radiation Measurements, v. 47, p. 201–209.

Gillespie, A.R., 1991, Testing a new climatic interpretation for the Tahoe glaciation, *in* Hall Jr., C.A., Doyle-Jones, V., and Widawski, B., eds, Natural History of Eastern California and High-Altitude Research, White Mountain Research Station Symposium Volume 3: Los Angeles, CA, University of California, p. 383–398.

Gillespie, A.R., Burke, R.M., Komatsu, G., and Bayasgalan, A., 2008, Late Pleistocene glaciers in Darhad Basin, northern Mongolia: Quaternary Research, v. 69, p. 169–187.

Gosse, J.C., and Phillips, F.M., 2001, Terrestrial in situ cosmogenic nuclides: theory and application: Quaternary Science Reviews, v. 20, p. 1475–1560.

Harris, I., Jones, P.D., Osborn, T.J., and Lister, D.H., 2014, Updated high-resolution grids of monthly climatic observations – the CRU TS3.10 Dataset: International Journal of Climatology, v. 34, p. 623–642.

Heyman, J., 2014, Paleoglaciation of the Tibetan Plateau and surrounding mountains based on exposure ages and ELA depression estimates: Quaternary Science Reviews, v. 91, p. 30–41.

Huntley, D.J., and Lamothe, M., 2001, Ubiquity of anomalous fading in K-feldspars and the measurement and correction for it in optical dating: Canadian Journal of Earth Sciences, v. 38(7), p. 1093–1106.

Janz, L., Feathers, J.K., Burr, G.S., 2015, Dating surface assemblages using pottery and eggshell: assessing radiocarbon and luminescence techniques in Northeast Asia: Journal of Archaeological Science, v. 57, p. 119–129.

Komatsu, G., Arzhannikov, S. G., Gillespie, A. R., Burke, R. M., Miyamoto, H., and Baker, V. R., 2009, Quaternary paleolake formation and cataclysmic flooding along the upper Yenisei River: Geomorphology, v. 104, p. 143–164.

Koppes, M., Gillespie, A.R., Burke, R.M., Thompson, S.C., and Stone, J., 2008, Late Quaternary glaciation in the Kyrgyz Tien Shan: Quaternary Science Reviews, v. 27, p. 846–866. doi:10.1016/j.quascirev.2008.01.009

Lal, D., 1991, Cosmic ray labeling of erosion surfaces: in situ nuclide production rates and erosion models: Earth and Planetary Science Letters, v. 104, p. 424–439.

Lifton, N.A., Bieber, J.W., Clem, J.M., Duldig, M.L., Evenson, P., Humble, J.E., and Pyle, R., 2005, Addressing solar modulation and long-term uncertainties in scaling in situ cosmogenic nuclide production rates: Earth and Planetary Science Letters, v. 239, p. 140–161.

Meierding, T.C., 1982, Late Pleistocene glacial equilibrium-line in the Colorado Front Range: a comparison of methods: Quaternary Research, v. 18, 289–310.

Mitchell, T. D., and Philip, D. J., 2005, An improved method of constructing a database of monthly climate observations and associated high resolution grids: International Journal of Climatology, v. 25, p. 693–712.

Nichols, K.K., Bierman, P.R., Foniri, W.R., Gillespie, A.R., Caffee, M., and Finkel, R., 2006, Dates and rates of arid region geomorphic processes: GSA Today, v. 16, no. 8, p. 4–11. doi: 10.1130/GSAT01608.1.

Prescott, J.R., and Hutton, J.T., 1994, Cosmic ray contributions to dose rates for luminescence and ESR dating: Large depths and long-term time variations: Radiation Measurements, v. 23, p. 497–500.

Prokopenko, A.A., Kuzmin, M.I., Williams, D.F., Gelety, V.F., Kalmychkov, G.V., Gvozdkov, A.N., and Solotchin, P.A., 2005, Basin-wide sedimentation changes and deglacial lake-level rise in the Hovsgol basin, NW Mongolia: Quaternary International, v. 136, p. 59–69.

Rother, H., Lehmkuhl, F., Fink, D., and Nottebaum, V., 2014, Surface exposure dating reveals MIS-3 glacial maximum in the Khangai Mountains of Mongolia: Quaternary Research, v. 82, p. 297–308.

Rupper, S., Roe, G., and Gillespie, A., 2009, Spatial patterns of Holocene glacier advance and retreat in Central Asia: Quaternary Research, v. 72, p. 337–346.

Sakai, A., Nuimura, T., Fujita, K., Takenaka, S., Nagai, H., and Lamsal, D., 2015, Climate regime of Asian glaciers revealed by GAMDAM glacier inventory: The Cryosphere, v. 9, p. 868–880.

Stone, J., 2000, Air pressure and cosmogenic isotope production: Journal of Geophysical Research, v. 105, no. 23, p. 753–23,759.

Wintle, A.G., and Murray, A.S., 2006, A review of quartz optically stimulated luminescence characteristics and their relevance in single-aliquot regeneration dating protocols: Radiation Measurements, v. 41, p. 369–191.